Research Article

Nano Research
2020, 13(6): 1564–1570

ISSN 1998-0124 CN 11-5974/O4
https://doi.org/10.1007/s12274-020-2771-3

Batch synthesis of transfer-free graphene with wafer-scale uniformity

Bei Jiang[1,§], Qiyue Zhao[2,§], Zhepeng Zhang[1], Bingzhi Liu[1], Jingyuan Shan[1], Liang Zhao[3], Mark H. Rümmeli[3], Xuan Gao[4], Yanfeng Zhang[1], Tongjun Yu[2], Jingyu Sun[3,4] (✉), and Zhongfan Liu[1,4] (✉)

[1] *Center for Nanochemistry (CNC), Beijing Science and Engineering Center for Nanocarbons, College of Chemistry and Molecular Engineering, Peking University, Beijing 100871, China*
[2] *State Key Laboratory for Artificial Microstructures and Mesoscopic Physics, School of Physics, Peking University, Beijing 100871, China*
[3] *College of Energy, Soochow Institute for Energy and Materials Innovations (SIEMIS), Key Laboratory of Advanced Carbon Materials and Wearable Energy Technologies of Jiangsu Province, Soochow University, Suzhou 215006, China*
[4] *Beijing Graphene Institute (BGI), Beijing 100095, China*
[§] *Bei Jiang and Qiyue Zhao contributed equally to this work.*

Received: 19 September 2019 / **Revised:** 4 March 2020 / **Accepted:** 22 March 2020

ABSTRACT

Scalable synthesis of transfer-free graphene over insulators offers exciting opportunity for next-generation electronics and optoelectronics. However, rational design of synthetic protocols to harvest wafer-scale production of directly grown graphene still remains a daunting challenge. Herein we explore a batch synthesis of large-area graphene with wafer-scale uniformity by virtue of direct chemical vapor deposition (CVD) on quartz. Such a controllable CVD approach allows to synthesize 30 pieces of 4-inch graphene wafers in one batch, affording a low fluctuation of optical and electrical properties. Computational fluid dynamics simulations reveal the mechanism of uniform growth, indicating thermal field and confined flow field play leading roles in attaining the batch uniformity. The resulting wafer-scale graphene enables the direct utilization as key components in optical elements. Our method is applicable to other types of insulating substrates (e.g., sapphire, SiO_2/Si, Si_3N_4), which may open a new avenue for direct manufacture of graphene wafers in an economic fashion.

KEYWORDS

graphene, batch synthesis, direct chemical vapor deposition (CVD), uniformity, wafer-scale, confined flow

1 Introduction

Wafer-size uniform graphene over insulators is of paramount importance for next-generation electrical, optical, and chemical applications [1–6]. A vivid example is pertaining to graphene on quartz substrate, which enables the direct integration of neutral density filter (NDF) devices for use in practical photography, benefiting from the linear and uniform absorption of visible light [7, 8]. The scalable availability of graphene wafers is a prerequisite to fulfill their wide potentials [1]. Along this line, batch synthesis on insulating substrates is imperative.

Amongst various graphene preparation techniques including mechanical/liquid exfoliation [9–11], chemical reduction of graphene oxides [12, 13], epitaxy on SiC [14], and chemical vapor deposition (CVD) [15, 16], the latter two are deemed to be feasible for the synthesis of wafer-scale graphene [17, 18]. As compared to the CVD route, epitaxy growth on SiC deals with a higher cost and more harsh operation conditions, rendering it unfavorable for the batch preparation [19]. CVD has a potential to grow large-area graphene with wafer-scale uniformity in an economic and mild fashion, as prevailed by effective synthesis over metals [20, 21]. Nevertheless, the inevitable procedures for transferring graphene off the metals onto the target insulators could be tedious and destructive, in turn not suitable for batch production [22]. In this sense, the direct and scalable CVD growth holds promise for the batch preparation of transfer-free graphene wafers, but this has not yet been realized thus far.

In a conventional CVD route for the growth of graphene on insulators, the insulating substrates normally lay flat within a horizontal tube furnace; additionally, the synthesis also heavily relies upon atmospheric pressure CVD (APCVD) conditions [22–24]. In this respect, the concentration of active carbon species cannot be easily tailored from upstream to downstream in the ambient pressure, resulting in inhomogeneous graphene coating along the direction of gas flow for these horizontally-placed samples [25]. This issue needs to be addressed for the case of batch synthesis to ensure viable uniformity and reproducibility [1]. On one hand, facing the substrate perpendicular to the direction of gas flow [26] might be helpful to re-distribute the carbon concentration and mitigate the inhomogeneity of obtained films. On the other hand, lowering the system pressure in combination with employing easily decomposed carbon precursor has proven successful to attain 25-inch-long uniform graphene glass sample [25]. With full consideration of these aspects, we develop herein a methodology inspired by advances from semiconductor industry for the batch synthesis of transfer-free graphene directly on quartz affording wafer-scale uniformity. The vertically aligned placement of substrates and the employment of ethanol precursor under low-pressure CVD (LPCVD) conditions create a confined flow field, allowing the production of 30 pieces of 4-inch graphene wafers in one batch.

Address correspondence to Zhongfan Liu, zfliu@pku.edu.cn; Jingyu Sun, sunjy86@suda.edu.cn

The excellent graphene uniformity of single wafer and entire batch is verified by a wide suite of characterizations. In addition, computational fluid dynamics (CFD) simulations [27, 28] on the gas velocity, thermal field distribution and mixed gas density further disclose the advancement of our route in the batch production of graphene wafers. As such, batch synthesis can be achieved by modulating comprehensive growth parameters and wafer intervals in the periodical alignment. The transmittance of graphene wafers can be highly uniform, affording small fluctuation of 1% in single wafer and ±2% in a batch. As proof-of-concept demonstrations, the obtained graphene wafers are versatile enough to act as key components in NDF device integration. In further contexts, the present growth route can be easily amplified in terms of wafer sizes and types. This work marks a solid step forward for the scalable synthesis of wafer-scale graphene in a practical manner.

2 Experimental

2.1 CVD growth of graphene directly on quartz wafers

Commercially available 2-inch to 4-inch quartz wafers were erected perpendicular to the airflow direction with the aid of homemade substrate holders in a 6-inch horizontal CVD tube furnace. The intervals between the wafer samples were set at 5, 10, 15 and 20 mm. Typically, after air annealing at 1,000 °C for 30 min, graphene growth was performed at 1,050 to 1,080 °C and 2 kPa using 0–500 sccm Ar, 500–800 sccm H_2, and 350–750 sccm ethanol vapor for ca. 1–5 h. Ethanol vapor was pumped into the chamber by using a rotameter.

2.2 Characterizations

The as-grown graphene wafers were systematically characterized by optical microscopy (OM) (Nikon, LV100ND), scanning electron microscopy (SEM) (Thermo Fisher Scientific, FEI Quattro S, operating at 1–5 kV), helium ion microscopy (ORION NANOLAB, operating at 30 kV), Raman spectroscopy (Horiba, LabRAM HR Evolution, 532 nm laser excitation, 100× objective lens), ultraviolet–visible (UV–vis) transmittance spectroscopy (Perkin-Elmer Lambda 950 spectrophotometer), four-probe resistance measuring meter (CDE, ResMap 178), atomic force microscopy (AFM) (BRUKER Dimension Icon, working at a tapping mode). The atomically resolved transmission electron microscopy (TEM) investigations of graphene were conducted on a FEI Titan Themis TEM equipped with a monochromator and a C_s corrector for the primary objective lens. The electron acceleration voltage was 80 kV. An Au Quantifoil TEM grid was used for supporting the sample, onto which graphene film was transferred with the aid of polymethyl methacrylate coating. To carry out optical transmittance mapping of graphene wafers, as-synthesized samples were fixed on a homemade stainless-steel stage with the presence of holes (Φ 2 mm) with fixed coordinates. The transmittance of corresponding spots on the sample can be obtained from a portable transmittance detector.

2.3 CFD simulations

Based on finite volume method, the thermal field and flow field of the batch system were simulated using turbulence model, ideal gas assumption, and axisymmetric approximation. Note that herein the thermal conduction, radiation and convection processes were all considered. In the solid domain, there was a thermal insulating layer, resistance type heaters, a quartz tube and wafers. In the fluid domain, there were the air outside the tube and mixed gas inside the tube.

2.4 Fabrication and measurement of Hall devices

UV lithography (URE-2000/35) and reactive ion etching (RIE) with O_2 (Trion Technology Minilock III) were employed for graphene patterning with designed geometry on 4-inch graphene/quartz wafers. Upon patterning a polymethyl methacrylate (PMMA) mask (PMMA 950K A4 @ 4,000 rpm) by UV lithography, 5-nm Cr and 45-nm Au electrodes were deposited on the graphene samples by high vacuum resistance evaporation (ZHD 300). Electrical measurements at room temperature were performed at a vacuum probe station (Lakeshore TTP-4) with Tektronix Keithley Semiconductor Characterization System (Model 4200-SCS).

3 Results and discussion

As illustrated in Fig. 1(a), a 6-inch CVD tube furnace possessing three zones is employed to enable the batch synthesis of transfer-free graphene on 4-inch quartz wafers. Quartz wafers

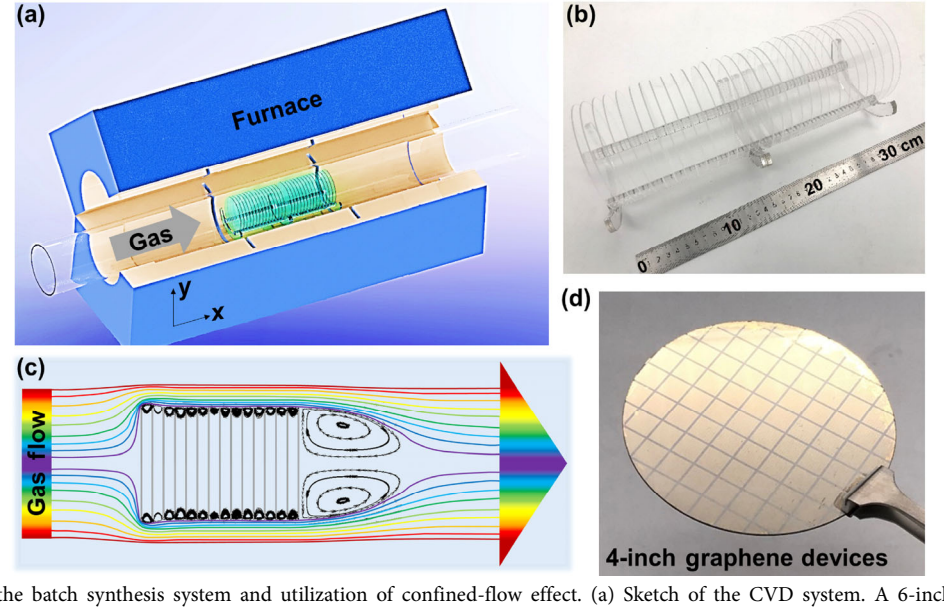

Figure 1 Design of the batch synthesis system and utilization of confined-flow effect. (a) Sketch of the CVD system. A 6-inch CVD tube furnace possessing three zones to accommodate quartz wafers in the second zone. (b) Photo of the quartz holders and quartz wafers in one batch. (c) Schematic of the confined-flow effect derived from the small vortices (marked as closed curves in black). (d) Photo of thus-fabricated 4-inch graphene devices.

as the growth substrates are vertically aligned in a systematical manner onto a home-made wafer holder, which is placed in the second zone within the furnace. Such a holder can support erected wafers with the diameter from 2 to 4 inch with tunable sample intervals (adjusted by an integral multiple of 5 mm). Note that the designed pedestal helps to mitigate the obstruction of gas flow (Fig. 1(b)), thereby ensuring a similar gas environment for the entire surface of a certain wafer. Such a design is evidently distinguished from the traditional holders employed in semiconductor industry. Upon employing the holder, 4-inch quartz wafers are homocentric with the quartz tube, and hence this system can be assumed to be axisymmetric, which is beneficial to conducting system simulations. Prior to the growth, the quartz wafers are subject to air annealing process. The batch synthesis of graphene wafers can be simply initiated by the introduction of vaporized ethanol precursor into the reaction chamber through a rotameter [25], accompanied by the controlled Ar and H_2 flows.

The gas environment (i.e., density, velocity) is of paramount importance toward the direct growth of graphene on quartz with wafer-scale uniformity. To probe the gas flow effect in detail within the designed system, CFD simulations were carried out. The 10-mm-interval scenario is shown below, and simulation results with other intervals are similar. Figure S1 in the Eleronic Supplementary Material (ESM) displays the distributions of the gas flow velocity (divided into two directions, x and y, as shown in Fig. 1(a)). It is evident that the velocities along both directions are near to zero between adjacent substrates, so that the boundary layers near the substrates except for the first and last substrates is not necessary to be considered. Under LPCVD, the concentration of active carbon species at bulk (C_g) and on substrate surface (C_s) have a relationship of $C_s \approx C_g$, and mass transport coefficient $h_g = D_g/\delta$ is related to boundary layer thickness δ (D_g is the diffusion coefficient of gas, which is higher under low pressure) [29].

$$C_s = \frac{h_g}{K_s + h_g} C_g \quad (1)$$

K_s is the surface reaction constant. Here, a lower δ means a higher h_g. Hence, the concentrations of active carbon species in gas phase and near substrate surface are quite similar. Specifically, the uniformity of C_g leads to the uniformity of C_s, and both surfaces in every interval are identical. Figure 1(c) further depicts the schematic diagram of gas flow for the system, highlighting the existence of small gas vortices marked by the black bubbles at the edges of wafers. These vortices lead to little gas exchange, affording a flow-confined effect, which creates an almost static region at the macroscopic level. Meanwhile, the vertical alignment of wafers ensures that such substrates are under identical CVD conditions, which is beneficial to attaining uniformity of batch synthesis. Additionally, combined with the analysis of the two surfaces in every interval, the quality and uniformity of graphene grown on both faces of a quartz wafer are almost identical. It is worth noting that there has to be a suitable separation distance between the array of substrates and the tube wall, because the viscous effect and heat conduction of the tube have a negative effect on the uniformity of batch synthesis.

Electrical tests (such as four-probe sheet resistance mapping and four-terminal resistance testing of Hall devices) can be utilized to characterize the uniformity of graphene. However, the data acquisition ranges of the two tests are different, and the spatial resolution of the latter is higher by three orders of magnitude. Thus-grown graphene wafers enable the direct fabrication of 4-inch graphene Hall devices (Fig. 1(d) and Fig. S2 in the ESM). The tested electrical performances verify the wafer-scale uniformity of directly-formed graphene (Fig. S3 in the ESM).

Exhaustive characterizations pertaining to the batch uniformity of directly grown graphene wafers were firstly demonstrated. As for large-sized graphene wafers, the uniformity could be evaluated by visual inspection, optical microscopy, Raman spectroscopy, and sheet resistance mapping. Specially, the uniformity of graphene on quartz can also be characterized by visible light transmittance mapping, benefiting from the high light transmission of quartz and linear absorption property of graphene. Figure 2(a) presents a photograph of 30 pieces of 4-inch graphene/quartz wafers prepared in one batch (with an interval of 10 mm). The samples from upper left to lower right within the photo correspond to those from upstream to downstream in the batch growth system. Obviously, the differences in appearance between the samples are difficult to be distinguished by the naked eye, suggesting favorable batch uniformity at a macroscopic level. Upon setting the transmittance range of each map to be the same, the batch uniformity can be simply reflected by comparing the map colors (Fig. 2(b) inset). As such, the average transmittance of single wafer (single side) was quantified, as indicated by the black short lines in Fig. 2(b). These values fall within a range from 92% to 96%, with small fluctuations (1%) of each sample (marked in red). Figure 2(c) shows typical Raman spectra of one batch graphene wafers. All the tested samples display prominent 2D peak intensities, accompanied by similar values of full width at half maximum, indicating the uniformity of graphene quality within the batch production. Moreover, average sheet resistances of batch samples are plotted, with error bars representing the data collected from 81 points on each sample (Fig. S4 in the ESM). It is noted that the samples at the batch front and end (Nos. 1, 2, 29 and 30) are slightly different from others in optical/electrical performances, owing to "edge effect" with respect to creating the growth environment for the batch system. Significantly, batch control can be achieved by adjusting a series of parameters, as revealed in Fig. 2(d). The radar map splitting into five directions demonstrates the relationships between the independent variables and growth targets. Intriguingly, graphene uniformity is negatively correlated with system pressure and almost irrelevant to system temperature (in the range of 1,050–1,080 °C), time and flow rate of carbon precursor. In fact, the negative correlation of pressure and batch uniformity introduced here refers to the bare CH_4-APCVD and ethanol-LPCVD routes instead of growth attempts via stepwise change of system pressures. Further analysis shows that uniformity is non-monotonically correlated with the interval.

As with the confirmation of batch uniformity, the synthesized graphene wafers were subject to a wide suite of characterizations to probe in detail the growth quality narrowing down to individual wafer. We selected two samples from two batches, in which one batch had a full coverage of graphene, and the other possessed incomplete film coverage, to show the wafer-scale uniformity and single crystal domain information, respectively. Note that each examined wafer was arbitrarily selected from one batch (i.e., 30 pieces of wafers). In terms of the wafer with full coverage of graphene, as shown in the digital photo in Fig. 3(a), there is no stark contrast difference over the entire 4-inch wafer. Accordingly, five representative zones marked in red (A–E) were inspected by Raman spectroscopy, with typical Raman spectrum demonstrated in Fig. S5(a) in the ESM. The intensity ratio of 2D and G band (I_{2D}/I_G) mappings in Fig. 3(a) reveal the uniformity of Raman signals in relatively large areas [30]. With respect to a typical

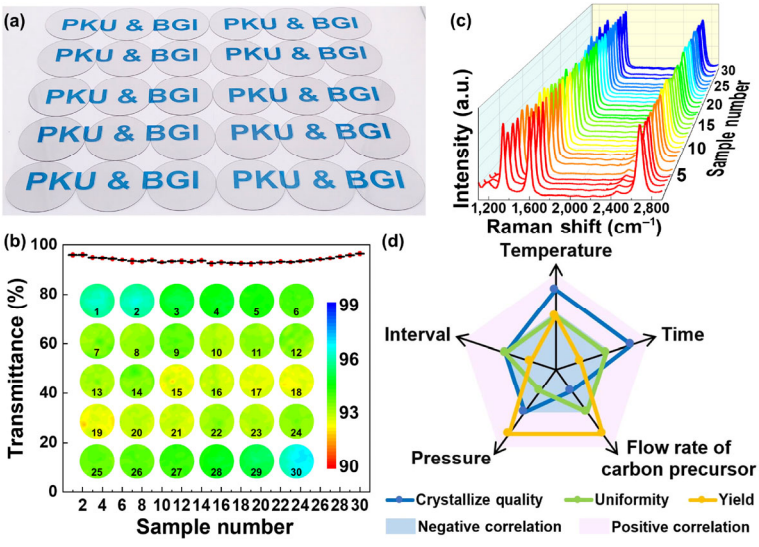

Figure 2 Characterizations of batch uniformity of 4-inch graphene wafers. (a) Photo of 30 pieces of as-synthesized graphene wafers in one batch. The samples from upper left to lower right within the photo correspond to those from upstream to downstream in the batch growth system. (b) Average transmittance spectra and mappings (inset) of these samples. The data fall within a range from 92% to 96%, with small fluctuation (1%) of every sample (marked in red). (c) Raman spectra of these wafers with normalized G peak, displaying prominent 2D peak intensities, accompanied by similar values of full width at half maximum. Growth conditions: 4-inch quartz wafers, 1,050 °C, 2 kPa, Ar/H_2/ethanol vapor = 500/500/500 sccm, 2 h. (d) Radar map with 5 directions demonstrating the relationships between growth targets and variables. The junction of negative and positive correlation represents independence or non-monotonicity.

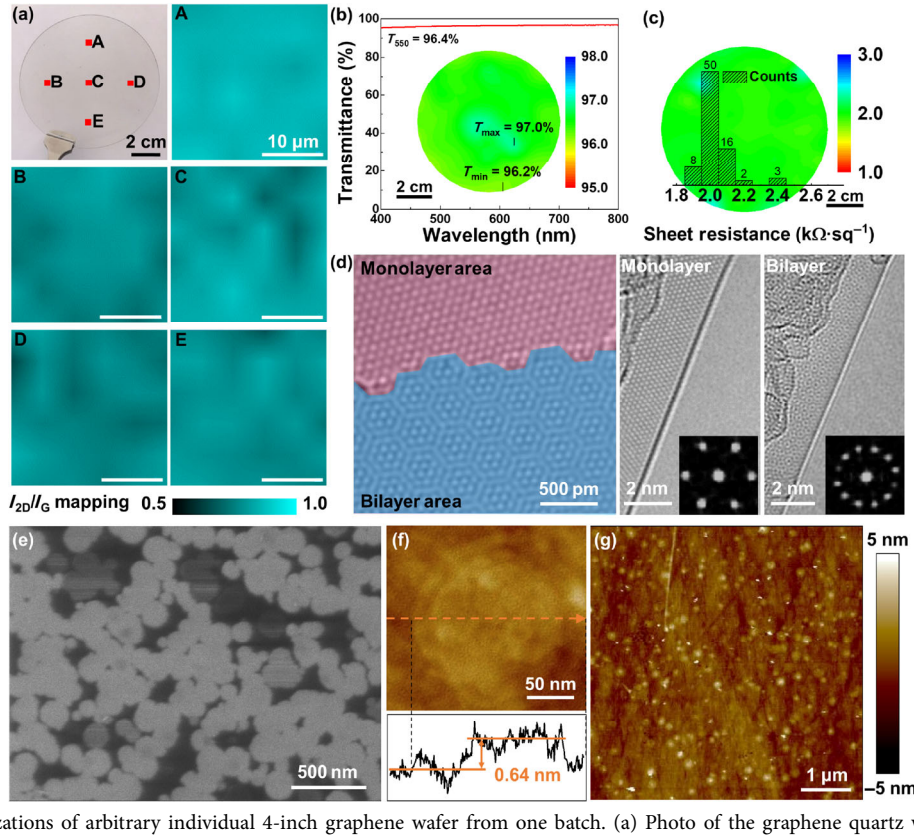

Figure 3 Characterizations of arbitrary individual 4-inch graphene wafer from one batch. (a) Photo of the graphene quartz wafer and corresponding I_{2D}/I_G Raman mappings. (b) Transmittance spectrum and relevant mapping of this sample. The optical transmittance at the wavelength of 550 nm harvests 96.4%. The mapping shows an extremely low transmittance fluctuation ratio of ca. 0.8% for the single side of graphene wafer. (c) Sheet resistance map and corresponding statistics. The uniform distribution of green color implies a high degree of graphene uniformity with an average sheet resistance value of 2.0 kΩ·sq^{-1}. (d) Atomically-resolved TEM images of the edges of graphene monolayer and bilayer regions. (e) Helium ion microscopy image of the near-circular single crystal domains of graphene. (f) AFM height image of a single crystal graphene domain. (g) AFM image of the graphene film on quartz. Growth conditions: 4-inch quartz wafers, 1,080 °C, 2 kPa, Ar/H_2/ethanol vapor = 0/800/350 or 0/800/400 sccm, 5 h.

Raman spectrum of the incompletely covered sample (Fig. S5(b) in the ESM), it displays a similar I_D/I_G ratio (approximately 2/3) as compared to the fully covered sample, but a markedly enhanced I_{2D}/I_G ratio. Figure 3(b) displays the typical transmittance spectrum of the graphene film. Apparently, the optical transmittance at the wavelength of 550 nm harvests 96.4%, indicative of the predominant existence of monolayer/bilayer graphene [3]. To further reflect the excellent uniformity of

directly-grown graphene, wafer-scale transmittance mapping was acquired by characterizing 81 points with fixed coordinates, affording an extremely low transmittance fluctuation ratio of ca. 0.8% for the single side of graphene wafer (Fig. 3(b) inset). Especially, graphene at the edge site of wafers is still of high uniformity because there is no obvious change of gas density and thermal field. Figure 3(c) shows a sheet resistance map of such a wafer sample, where the uniform distribution of green color implies a high degree of graphene uniformity with an average sheet resistance value of 2.0 kΩ·sq^{-1}. In further contexts, the crystalline quality of grown graphene was analyzed with the aid of a low-voltage, atomically-resolved TEM. Figure 3(d) (left panel) captures the lattice of graphene with co-existed monolayer and bilayer areas (marked as red and blue colors, respectively). The right panel presents the high-magnification TEM image and corresponding diffraction patterns of the edges of monolayer and bilayer regions. Supplementary TEM images in Fig. S6 in the ESM show the hexagonal atomic arrangements of a single crystal domain in the incompletely covered sample. Additionally, typical SEM image shows full coverage of graphene films on the substrate, with barely no substrate exposed and a few secondary nuclei on the top (Fig. S7 in the ESM). Further image analysis indicates that the area with the dark contrast corresponds to the bare quartz substrate, and the region with the light contrast is the first layer of grown graphene. It can be seen that most of the areas exhibit the same light contrast, so that the surface of the sample is covered by a single layer of graphene. To further estimate the single domain size of as-grown graphene, sub-monolayer coverage is selectively realized. Figure 3(e) displays a helium ion microscopy image of the near-circular-shaped crystal domains of graphene. This can also be witnessed from the AFM height image (Fig. 3(f)). Moreover, AFM observation of the graphene film on quartz reveals the flat surface nature of the as-prepared graphene sample (Fig. 3(g)). The discrete white spots correspond to bilayer areas, in good agreement with the SEM image. Taken together, these results disclose the wafer-scale uniformity of our batch synthesis.

To further investigate the effects of gas density and growth temperature on the wafer-scale uniformity of graphene, CFD simulations based on finite volume method [31] were systematically performed to guide us to better implement the batch control. The thermal field and flow field of the designed batch system were simulated using turbulence model [32], ideal gas assumption [33], and axisymmetric approximation [34]. Firstly, the distributions of mixed gas density under AP and LP were examined using the identical 5-mm interval (Figs. 4(a) and 4(b)). It is evident that the gas density between every two pieces of erected quartz wafers under LP distributes more uniformly as compared to that under AP, indicating that LP condition is more suitable for our batch preparation system. In further contexts, when the intervals were adjusted to 10, 15, and 20 mm, the gas density can still maintain in a uniform fashion (Fig. 4(b)). Although the mixed gas density in between the space of quartz wafers is much smaller than that outside, the vortices can trap the gas flow to accommodate the carbon active species in the high-temperature regions, guaranteeing the successful growth of graphene.

Thermal field is another key factor for the uniform growth of graphene due to the temperature dependence of precursor decomposition and active carbon diffusion. With the full consideration of thermal conduction, radiation and convection processes [35], erected quartz wafers and the confined gas can trap heat and generate a high-temperature region (Fig. S8 in the ESM). Specifically, the change of wafer intervals can exert a profound impact on the thermal conduction and radiation, thereby leading to the variation of thermal field. Figure 4(c) plots detailed parameters to draw a comparison of individual wafer uniformity and batch uniformity of thermal field between four LP systems, marked by 5-mm, 10-mm, 15-mm and 20-mm intervals, respectively. On one hand, to compare the temperature uniformity of every single wafer in four scenarios, ΔT_0 is introduced, which is the maximum temperature difference ($T_{0,\max} - T_{0,\min}$) for an individual wafer. In addition, the mean value and standard deviation (SD) of ΔT_0 represent the average level and convergence of data, respectively. Therefore, (mean value ± SD) denotes the temperature uniformity of every single wafer in one batch. As such, the system with 10-mm interval possesses the smallest mean value of ΔT_0 and (mean value ± SD), suggesting its superior thermal uniformity to those of the other three systems. On the other hand, SD of central temperature (T) among all wafers in a system reflects batch temperature uniformity. Indeed, the sample interval exerts a significant impact on the fluctuations of single wafer temperature and entire batch temperature, in turn influencing the uniformity of graphene wafers (Fig. S9 in the ESM). Based on ideal gas assumption and flow-confined effect, a uniform thermal field

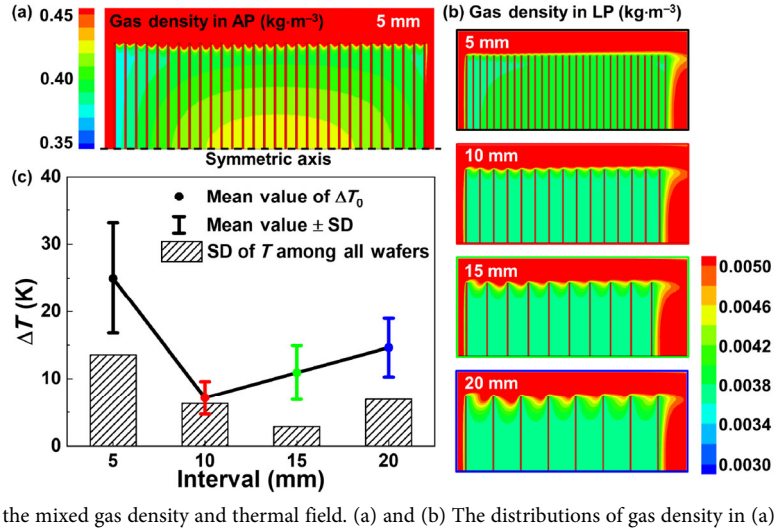

Figure 4 CFD simulations of the mixed gas density and thermal field. (a) and (b) The distributions of gas density in (a) AP with 5-mm interval and (b) LP with different intervals. (c) Mean value and SD of the maximum temperature difference ΔT_0 ($T_{0,\max} - T_{0,\min}$) for every wafer and SD of central temperature (T) among all wafers with a certain interval. The system with 10-mm interval possesses the smallest mean value of ΔT_0 and (mean value ± SD), suggesting its superior thermal uniformity to those of the other three systems. The SD of T reflects batch temperature uniformity.

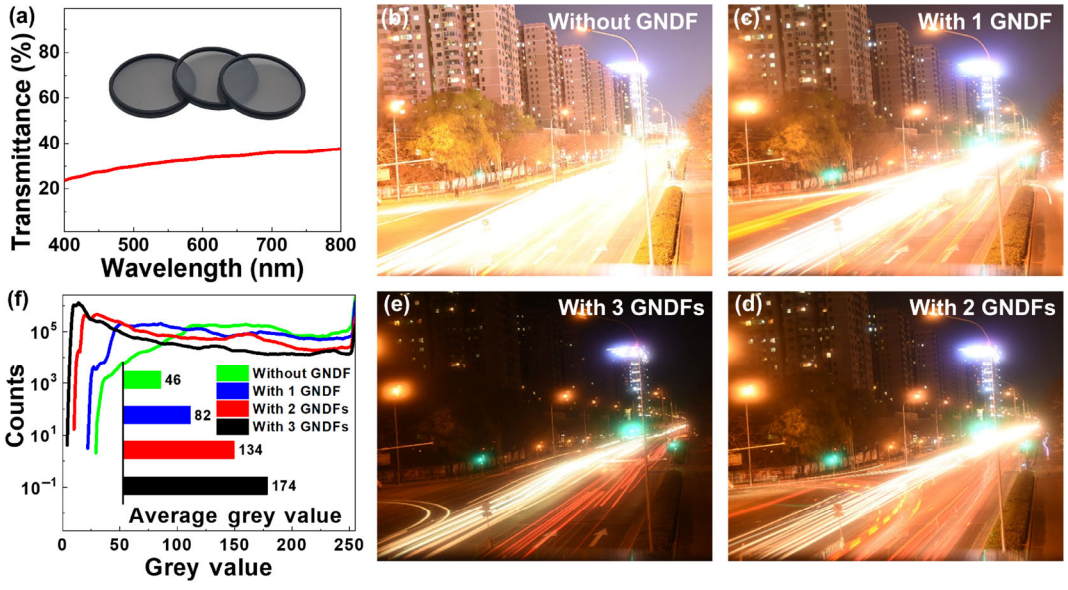

Figure 5 Applications of wafer-scale graphene as NDFs. (a) The transmittance spectrum of a GNDF in visible-light region (inset: photo of the as-fabricated GNDFs). Every GNDF consists of a piece of direct-CVD-derived graphene wafer sealed by two layers of transparent polymeric membranes. (b)–(e) Photos taken with/without GNDFs. The GNDFs lead to the avoidance of overexposure. (f) The counts of grey-value points and the mean grey values of the four photos in (b)–(e). Advanced filtering effect contributes to generally lower grey values.

would lead to building-up a uniform gas density. Therefore, the growth of graphene is much more uniform in this static region. Comprehensively tuning the sample intervals, system pressures and thermal fields would allow the realization of batch synthesis of transfer-free graphene with wafer-scale uniformity.

Meanwhile, the as-designed synthetic system has excellent batch reproducibility (Fig. S10 in the ESM). Accordingly, as-synthesized graphene/quartz wafers with large-scale uniformity have great implications in versatile application sectors. For instance, NDFs enable the non-selective decrease of light intensity at certain wave bands, and thus find wide usage in optical instruments, including camera, medical photodetector, clinical analysis, chemical detection, and electronic imaging system. In this respect, direct graphene formation on quartz wafer would afford a linear and uniform light absorption (via graphene) covering a wide spectral range, giving rise to the design of graphene NDFs (GNDFs) [7, 8, 36]. Figure 5(a) shows the visible-light transmittance spectrum of our GNDF, with the inset displaying real photos of the GNDF samples (Φ70 wafer size). Note that each GNDF consists of a piece of direct-CVD-derived graphene wafer sealed by two layers of transparent polymeric membranes. As a proof-of-concept demonstration, GNDFs can be directly inserted into a single lens reflex camera for photo shooting. As shown in Figs. 5(b)–5(e), the digital photos taken with/without the employment of GNDFs comparatively manifest the conspicuous filtering effect of the GNDF, leading to the avoidance of overexposure. Note that the addition of GNDFs would result in enhanced filtering effect. In response, Fig. 5(f) plots the distributions of grey values of these four photos, with the mean values presented as the inset. It is known that advanced filtering effect contributes to generally lower grey values, which accords well with the foregoing tests in the presence of our GNDFs.

4 Conclusions

In summary, we have demonstrated batch synthesis of transfer-free graphene on quartz accomplishing wafer-scale uniformity. The uniformity of as-synthesized graphene films on 4-inch-sized wafers is systematically verified by various characterization techniques. Guided by CFD simulations, small gas vortices and the confined-flow effect in the designed system have been disclosed, creating an almost static region at the macroscopic level and leading to attaining excellent uniformity of graphene in one batch. The adjustment of sample intervals influences the distribution of thermal field and gas density, thereby dictating the uniformity of directly grown graphene in a batch manner. Amongst emerging application sectors, thus-derived graphene wafers find uses as functional GNDFs. Essentially, the present work offers a reliable approach for the batch production of transfer-free graphene on wafer-size insulators, promoting the application of graphene into reality.

Acknowledgements

This work was financially supported by the National Basic Research Program of China (No. 2016YFA0200103), the National Natural Science Foundation of China (Nos. 61527814, 51702225, 51432002, 61474109, 51290272, 51502007, 11474274, and 51672007), the National Equipment Program of China (No. ZDYZ2015-1), Beijing Municipal Science and Technology Planning Project (Nos. Z181100004818002 and Z191100000819004), and Beijing Natural Science Foundation (No. 4182063).

Supplementary Material: Supplementary material (further simulation results and sample characterizations) is available in the online version of this article at https://doi.org/10.1007/s12274-020-2771-3.

References

[1] Lin, L.; Peng, H. L.; Liu, Z. F. Synthesis challenges for graphene industry. *Nat. Mater.* **2019**, *18*, 520–524.

[2] Zhu, Y. W.; Murali, S.; Cai, W. W.; Li, X. S.; Suk, J. W.; Potts, J. R.; Ruoff, R. S. Graphene and graphene oxide: Synthesis, properties, and applications. *Adv. Mater.* **2010**, *22*, 3906–3924.

[3] Bonaccorso, F.; Sun, Z.; Hasan, T.; Ferrari, A. C. Graphene photonics and optoelectronics. *Nat. Photonics* **2010**, *4*, 611–622.

[4] Loh, K. P.; Bao, Q. L.; Eda, G.; Chhowalla, M. Graphene oxide as a chemically tunable platform for optical applications. *Nat. Chem.* **2010**, *2*, 1015–1024.

[5] Lee, Y.; Bae, S.; Jang, H.; Jang, S.; Zhu, S. E.; Sim, S. H.; Song, Y. I.; Hong, B. H.; Ahn, J. H. Wafer-scale synthesis and transfer of graphene films. *Nano Lett*. **2010**, *10*, 490–493.
[6] Liu, M.; Yin, X. B.; Ulin-Avila, E.; Geng, B. S.; Zentgraf, T.; Ju, L.; Wang, F.; Zhang, X. A graphene-based broadband optical modulator. *Nature* **2011**, *474*, 64–67.
[7] Nair, R. R.; Blake, P.; Grigorenko, A. N.; Novoselov, K. S.; Booth, T. J.; Stauber, T.; Peres, N. M. R.; Geim, A. K. Fine structure constant defines visual transparency of graphene. *Science* **2008**, *320*, 1308.
[8] Xia, F. N.; Wang, H.; Xiao, D.; Dubey, M.; Ramasubramaniam, A. Two-dimensional material nanophotonics. *Nat. Photonics* **2014**, *8*, 899–907.
[9] Hernandez, Y.; Nicolosi, V.; Lotya, M.; Blighe, F. M.; Sun, Z. Y.; De, S.; McGovern, I. T.; Holland, B.; Byrne, M.; Gun'Ko, Y. K. et al. High-yield production of graphene by liquid-phase exfoliation of graphite. *Nat. Nanotechnol*. **2008**, *3*, 563–568.
[10] Novoselov, K. S.; Geim, A. K.; Morozov, S. V.; Jiang, D.; Zhang, C.; Dubonos, S. V.; Grigorieva, I. V.; Firsov, A. A. Electric field effect in atomically thin carbon films. *Science* **2004**, *306*, 666–669.
[11] Paton, K. R.; Varrla, E.; Backes, C.; Smith, R. J.; Khan, U.; O'Neill, A.; Boland, C.; Lotya, M.; Istrate, O. M.; King, P. et al. Scalable production of large quantities of defect-free few-layer graphene by shear exfoliation in liquids. *Nat. Mater*. **2014**, *13*, 624–630.
[12] Hirata, M.; Gotou, T.; Horiuchi, S.; Fujiwara, M.; Ohba, M. Thin-film particles of graphite oxide 1: High-yield synthesis and flexibility of the particles. *Carbon* **2004**, *42*, 2929–2937.
[13] Eda, G.; Fanchini, G.; Chhowalla, M. Large-area ultrathin films of reduced graphene oxide as a transparent and flexible electronic material. *Nat. Nanotechnol*. **2008**, *3*, 270–274.
[14] Berger, C.; Song, Z. M.; Li, X. B.; Wu, X. S.; Brown, N.; Naud, C.; Mayou, D.; Li, T. B.; Hass, J.; Marchenkov, A. N. et al. Electronic confinement and coherence in patterned epitaxial graphene. *Science* **2006**, *312*, 1191–1196.
[15] Reina, A.; Jia, X. T.; Ho, J.; Nezich, D.; Son, H.; Bulovic, V.; Dresselhaus, M. S.; Kong, J. Large area, few-layer graphene films on arbitrary substrates by chemical vapor deposition. *Nano Lett*. **2009**, *9*, 30–35.
[16] Wei, D. C.; Liu, Y. Q.; Wang, Y.; Zhang, H. L.; Huang, L. P.; Yu, G. Synthesis of n-doped graphene by chemical vapor deposition and its electrical properties. *Nano Lett*. **2009**, *9*, 1752–1758.
[17] Emtsev, K. V.; Bostwick, A.; Horn, K.; Jobst, J.; Kellogg, G. L.; Ley, L.; McChesney, J. L.; Ohta, T.; Reshanov, S. A.; Rohrl, J. et al. Towards wafer-size graphene layers by atmospheric pressure graphitization of silicon carbide. *Nat. Mater*. **2009**, *8*, 203–207.
[18] Deng, B.; Pang, Z. Q.; Chen, S. L.; Li, X.; Meng, C. X.; Li, J. Y.; Liu, M. X.; Wu, J. X.; Qi, Y.; Dang, W. H. et al. Wrinkle-free single-crystal graphene wafer grown on strain-engineered substrates. *ACS Nano* **2017**, *11*, 12337–12345.
[19] Novoselov, K. S.; Fal'ko, V. I.; Colombo, L.; Gellert, P. R.; Schwab, M. G.; Kim, K. A roadmap for graphene. *Nature* **2012**, *490*, 192–200.
[20] Li, X. S.; Cai, W. W.; An, J.; Kim, S.; Nah, J.; Yang, D. Y.; Piner, R.; Velamakanni, A.; Jung, I.; Tutuc, E. et al. Large-area synthesis of high-quality and uniform graphene films on copper foils. *Science* **2009**, *324*, 1312–1314.
[21] Zou, Z. Y.; Fu, L.; Song, X. J.; Zhang, Y. F.; Liu, Z. F. Carbide-forming groups IVB-VIB metals: A new territory in the periodic table for CVD growth of graphene. *Nano Lett*. **2014**, *14*, 3832–3839.
[22] Chen, J. Y.; Wen, Y. G.; Guo, Y. L.; Wu, B.; Huang, L. P.; Xue, Y. Z.; Geng, D. C.; Wang, D.; Yu, G.; Liu, Y. Q. Oxygen-aided synthesis of polycrystalline graphene on silicon dioxide substrates. *J. Am. Chem. Soc*. **2011**, *133*, 17548–17551.
[23] Sun, J. Y.; Chen, Y. B.; Priydarshi, M. K.; Chen, Z.; Bachmatiuk, A.; Zou, Z. Y.; Chen, Z. L.; Song, X. J.; Gao, Y. F.; Rümmeli, M. H. et al. Direct chemical vapor deposition-derived graphene glasses targeting wide ranged applications. *Nano Lett*. **2015**, *15*, 5846–5854.
[24] Sun, J. Y.; Chen, Z. L.; Yuan, L.; Chen, Y. B.; Ning, J.; Liu, S. W.; Ma, D. L.; Song, X. J.; Priydarshi, M. K.; Bachmatiuk, A. et al. Direct chemical-vapor-deposition-fabricated, large-scale graphene glass with high carrier mobility and uniformity for touch panel applications. *ACS Nano* **2016**, *10*, 11136–11144.
[25] Chen, X. D.; Chen, Z. L.; Jiang, W. S.; Zhang, C. H.; Sun, J. Y.; Wang, H. H.; Xin, W.; Lin, L.; Priydarshi, M. K.; Yang, H. et al. Fast growth and broad applications of 25-inch uniform graphene glass. *Adv. Mater*. **2017**, *29*, 1603428.
[26] Chen, Z. T.; Guo, X. L.; Zhu, L.; Li, L.; Liu, Y. Y.; Zhao, L.; Zhang, W. J.; Chen, J.; Zhang, Y.; Zhao, Y. H. Direct growth of graphene on vertically standing glass by a metal-free chemical vapor deposition method. *J. Mater. Sci. Technol*. **2018**, *34*, 1919–1924.
[27] Li, G.; Huang, S. H.; Li, Z. Y. Gas-phase dynamics in graphene growth by chemical vapour deposition. *Phys. Chem. Chem. Phys*. **2015**, *17*, 22832–22836.
[28] Feng, J. G.; Yan, X. X.; Zhang, Y. F.; Wang, X. D.; Wu, Y. C.; Su, B.; Fu, H. B.; Jiang, L. "Liquid knife" to fabricate patterning single-crystalline perovskite microplates toward high-performance laser arrays. *Adv. Mater*. **2016**, *28*, 3732–3741.
[29] Bhaviripudi, S.; Jia, X. T.; Dresselhaus, M. S.; Kong, J. Role of kinetic factors in chemical vapor deposition synthesis of uniform large area graphene using copper catalyst. *Nano Lett*. **2010**, *10*, 4128–4133.
[30] Cançado, L. G.; Jorio, A.; Ferreira, E. H. M.; Stavale, F.; Achete, C. A.; Capaz, R. B.; Moutinho, M. V. O.; Lombardo, A.; Kulmala, T. S.; Ferrari, A. C. Quantifying defects in graphene via Raman spectroscopy at different excitation energies. *Nano Lett*. **2011**, *11*, 3190–3196.
[31] Moukalled, F.; Mangani, L.; Darwish, M. *The Finite Volume Method in Computational Fluid Dynamics*; Springer: Cham, 2016.
[32] Shirzadi, M.; Mirzaei, P. A.; Naghashzadegan, M. Improvement of k-epsilon turbulence model for CFD simulation of atmospheric boundary layer around a high-rise building using stochastic optimization and Monte Carlo sampling technique. *J. Wind Eng. Ind. Aerod*. **2017**, *171*, 366–379.
[33] Ariafar, K.; Buttsworth, D.; Al-Doori, G.; Sharifi, N. Mixing layer effects on the entrainment ratio in steam ejectors through ideal gas computational simulations. *Energy* **2016**, *95*, 380–392.
[34] Gildfind, D. E.; Jacobs, P. A.; Morgan, R. G.; Chan, W. Y. K.; Gollan, R. J. Scramjet test flow reconstruction for a large-scale expansion tube, Part 2: Axisymmetric CFD analysis. *Shock Waves* **2018**, *28*, 899–918.
[35] Dobbins, R. R.; Hall, R. J.; Cao, S.; Bennett, B. A. V.; Colket, M. B.; Smooke, M. D. Radiative emission and reabsorption in laminar, ethylene-fueled diffusion flames using the discrete ordinates method. *Combust. Sci. Technol*. **2015**, *187*, 230–248.
[36] Currie, M.; Gaskill, D. K. Broadband absorptive neutral density optical filter. U.S. Patent 20160041318A1, February 11, 2016.